IDENTIFICATION OF THERMAL BOUNDARY CONDITIONS AND THERMO-METALLURGICAL BEHAVIOUR OF X10CrMoVNb9-1 STEEL DURING SIMPLE TIG WELDING TESTS

Guilhem Roux, René Billardon

IDENTIFICATION OF THERMAL BOUNDARY CONDITIONS AND THERMO-METALLURGICAL BEHAVIOUR OF X10CrMoVNb9-1 STEEL DURING SIMPLE TIG WELDING TESTS

G.-M. ROUX[1,2] and R. BILLARDON[1]

[1] *LMT-Cachan (E.N.S. de Cachan / CNRS (UMR8535) / University Paris 6) 61, Avenue du Président Wilson,, 94235 Cachan Cedex, France*

[2] *CEA (DEN/DANS/DM2S/SEMT/LM2S, France)*

ABSTRACT

To validate the thermo-metallurgical models that are used during finite element simulations of multi-pass TIG welding, two simple experiments - called "disk-spot" and "disk-cycle" TIG welding tests- have been designed. A procedure has been developed to identify the thermal boundary conditions that are imposed to the specimen during these experiments. These boundary conditions include the heat source that is equivalent to the TIG torch as well as the heat flux by convection (-radiation) at the surface of the specimen. A thermo-metallurgical model has been built and identified to represent most important phase changes occurring in a X10CrMoVNb9-1 martensitic steel -also known as ASTM A387 or T91 steel- during the welding process. The results of the thermo-metallurgical analysis of a "disk-spot" TIG mono-pass welding test without metal deposit is compared with experimental observations.

INTRODUCTION

The nominal temperature in the pressure vessels of future nuclear reactors -or so-called Very High Temperature Reactors using gas coolant at low pressure- should be around 450 °C. Because of its microstructural stability at such a temperature, X10CrMoVNb9-1 martensitic steel -also known as ASTM A387 or T91 steel- is considered as a promising candidate material for these structures. Since, the manufacturing process of such thick pressure vessels will most probably involve TIG multi-pass welding, different studies are presently in progress in different laboratories to develop reliable tools for the failure assessment of multi-pass weld joints in structures made of X10CrMoVNb9-1 martensitic steel.

The work presented herein is part of a study the aim of which is to develop finite element simulations of TIG multi-pass welding to predict the residual stresses induced by the process in the vicinity of welded joints in thick structures made of X10CrMoVNb9-1

martensitic steel. Since the accuracy of such complex thermo-metallo-mechanical finite element analyses strongly depends on many inputs, two simple experiments, that are called "disk-spot" and "disk-cycle" TIG welding tests, have been designed to validate the numerical tool that is currently in development.

The thermal boundary conditions that are applied to the specimen during a disk-spot TIG welding test without metal deposit are identified in the first part of this paper. The model that is proposed to model the thermo-metallurgical behaviour of X10CrMoVNb9-1 steel during the welding process is discussed and identified in the second part of this paper. The third and last part of this paper is dedicated to the first comparisons between experimental observations and results of thermo-metallurgical numerical simulations of a disk-spot TIG mono-pass welding test without metal deposit.

THERMAL BOUNDARY CONDITIONS

DISK-SPOT AND DISK-CYCLE TIG WELDING TESTS

The development of a reliable finite element tool to simulate TIG multi-pass welding requires a validation procedure including comparisons between experimental results obtained during well controlled tests and the numerical results of the corresponding simulations. Such structural analyses involve so many different thermo-metallo-mechanical aspects that the complete validation procedure of the predictive capabilities of the numerical tool must be a multi-step process, the first steps corresponding to problems of limited complexity. The so-called disk-spot TIG welding test has been designed to validate simulations of TIG mono-pass welding without metal deposit. The so-called disk-cycle TIG welding test has been designed to validate simulations of TIG mono- or multi-pass welding without or with metal deposit.

The disk-spot TIG welding test consists in heating in its centre a circular disk with a TIG spot torch without filler material. The disk rests on three point supports that are made of long ceramic pins in order to minimize contact heat conduction as well as spurious radiation effects. As shown on Fig. 1, different thermocouples and displacement sensors can be used to measure the temperature and the vertical or radial displacements at different points of the disk. A global view of the experimental set up is given in Fig. 2 where the disk is 8 mm thick and 50 mm in diameter.

The disk-cycle TIG welding test can be performed on the same experimental set-up, first, by locating the TIG torch at a given non zero radius and then, by controlling the horizontal displacement of the torch so that its trajectory is a circle. The first circle corresponds to the first welding pass. After a full circle has been completed, the following circles correspond to successive passes. Disk-cycle TIG welding tests can be performed without or with filler material.

The TIG source used for the experiments that are presented in this paper is an automatic Polysoude© TIG source and the welding process parameters used for these experiments are given in Tab. 1. Because of the low weight of the disk, "sticking" between the disk and the electrode must be avoided and non-contact priming is obtained by using high frequency current.

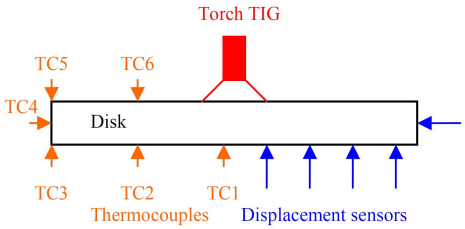

Fig. 1 Disk-spot TIG welding tests.

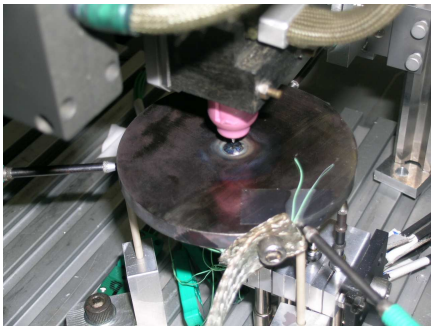

Fig. 2 Experimental set up.

Tab. 1 Welding process parameters.

Intensity I, Voltage U	100 A, 10 V
Diameter of the torch nose	12 or 16 mm
Electrode sharpening	30°
Length of the electrode	10 mm
Gas	12 l/min of argon

IDENTIFICATION PROCEDURE

The TIG torch -without filler material- used for the experiments discussed herein is modelled as a surfacic heat source of given analytical form. The heat flux at the surface of the specimen is modelled by a temperature dependent convection-radiation coefficient. In the following, these thermal boundary conditions are identified while assuming that the thermal properties of the welded material are known.

A typical plot of the evolution during heating of the specific heat, thermal conductivity and density of the base material used for the experiments presented herein is given in Fig. 3. One can notice the non-monotonous evolution of the thermal properties due to a solid-solid phase change that will be discussed in next section of this paper.

During heat transfer analyses, it is common to model, as a first approximation, the heat flux at the surface of solids as:

$$q = -h(T - T_\infty) \tag{1}$$

where h, T and T_∞ respectively denote the convection-radiation coefficient, the local surface temperature and the temperature in the atmosphere "far" from the solid. The convection-radiation coefficient obviously depends on the nature of the surface, its local temperature T and many environmental factors.

Among other analytical models, it has been chosen to represent the TIG torch -without filler material- as a surfacic heat source represented by a truncated infinite Gaussian

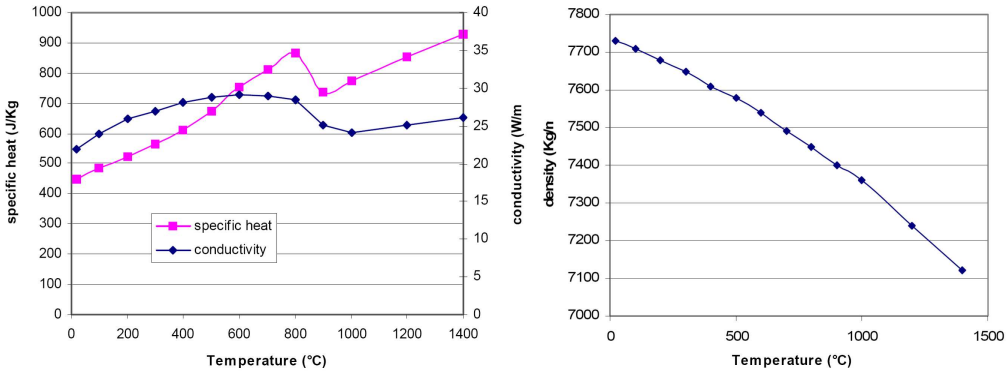

Fig. 3 Resistance spotwelding principle.

function:

$$P_S = Q\exp\left(-3\frac{r^2}{r_0^2}\right) \qquad \text{with} \qquad 0 \leq r \leq r_{Max} \tag{2}$$

where Q, r, r_0 and r_{Max} respectively denote the intensity of the TIG torch, the current radius and characteristic radii of the torch -measured from the axis of the torch.

These choices imply that the thermal boundary conditions that are imposed to the disk during the welding process are defined by the values of the variable convection-radiation coefficient h at any point on the surface of the disk as well as the values of the parameters of the heat source, viz. Q, r_0 and r_{Max}.

A sensitivity analysis has shown that the accuracy of the heat transfer numerical analysis of this experiment strongly depends on the convection-radiation coefficient [2]. For instance, it can be shown that the influence on the surface temperature far from the centre of the disk on the surface opposite to the TIG torch of geometric heat source parameter r_0 is negligible compared to the influence of convection-radiation coefficient h.

However, to simplify the identification process of the thermal boundary conditions -from a limited number of local temperature measurements- it is proposed to assume that:

- the convection-radiation coefficient is solely temperature dependant -for given material and environment-;
- the value of r_{Max} can be a priori fixed -for given welding parameters.

Hence, the process is restricted to the identification of the relationship $h(T)$ -that is supposed to be valid at any point on the surface of the disk- and of the values of parameters Q and r_0 (see Fig. 4). In practise, the identification procedure that has been applied is a two-step process.

The first step consists in the analysis of the cooling of the disk after its heating in an oven up to a uniform temperature of 800 °C and the identification of the evolution of the convection-radiation coefficient from 700 °C to room temperature.

The inverse identification of the evolution of the convection-radiation coefficient has been performed by using a Levenberg-Marquardt gradient minimization algorithm [3-4] and Cast3M [5] 2-D axisymmetric finite element heat transfer analyses. It consists in the minimization of the following quadratic function of measured and numerically predicted temperatures, respectively denoted by T_e and T_n, at given control points -of radius r - and given time steps t:

$$J = \sqrt{\frac{1}{M_0 M_t} \sum_{1}^{M_0} \sum_{1}^{M_t} \left[T_e(r,t) - T_n(r,t)\right]^2} \tag{3}$$

where M_0 and M_t respectively denote the number of control points and the number of time steps. The identified temperature evolution of coefficient h -while assuming $T_\infty = 20$ °C - is given in Tab. 2.

Tab. 2 Values of the convection-radiation coefficient h to be associated to $T_\infty = 20$ °C as identified from the cooling of an oven heated disk.

T [°C]	20	100	200	300	400	500	600	700
h [W/m^2]	10.026	12.765	16.23	21.754	27.754	36.127	42.423	51.188

To minimize the number of parameters to be identified, it is assumed that the evolution of convection-radiation coefficient h at temperatures higher than 700 °C can be interpolated from its values up to 700 °C and its value at a single higher temperature, say 1400 °C.

However, it appears that the non-convexity of the problem does not allow the inverse identification of the value of convection-radiation coefficient h(1400 °C) together with the heat source parameters Q and r_0, from the heat transfer analysis of a single experiment. Conversely, convergence of the minimization algorithm can be achieved by coupling the analyses of two disk-spot tests that are performed with different TIG torches, i.e. with different heat source parameters Q and r_0, whereas the heat flux at the surface of the disk is supposed to be controlled by the same temperature evolution of the convection-radiation coefficient $h(T)$.

Hence, the second step of the identification procedure consists in the inverse identification of the convection-radiation coefficient h(1400 °C) together with the two sets of parameters (Q_1, r_{01}) and (Q_2, r_{02}) that define the heat sources respectively associated to TIG torches that are chosen 12 and 16 mm in diameter (see Fig. 5). The same gradient minimization algorithm has been used -with identical sets of time steps t and control points of radius r for both experiments-.

The values gathered in Tab. 3 illustrate the convergence of the minimization algorithm during the second step of the identification procedure and the final results of this identification procedure are given in Fig. 6.

The quality of this identification is illustrated by the comparison that is given in Fig. 7 (for the disk-spot TIG welding test with a ø16 mm TIG torch) of the experimentally mea-

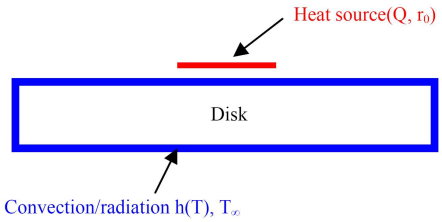

Fig. 4 Thermal boundary conditions during disk-spot TIG welding tests.

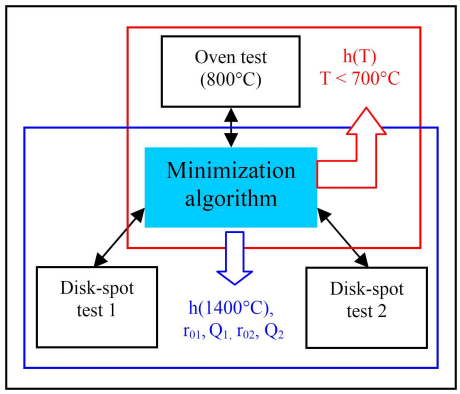

Fig. 5 Two-step identification procedure of thermal boundary conditions.

Tab. 3 Values of the heat sources parameters and convection-radiation coefficient as identified from two disk-spot tests.

	1st test (ø12 mm TIG torch)		1st test (ø16 mm TIG torch)		h [W/m^2] at 1400 °C
	Q_1 [W]	r_{01} [10^{-3} m]	Q_2 [W]	r_{02} [10^{-3} m]	
Initial values 1	500	10	500	10	100
Identified values 1	865.65	1.09154	816.42	3.95930	161.84
Initial values 2	800	1	800	1	20
Identified values 2	865.66	1.09155	816.43	3.95933	161.86

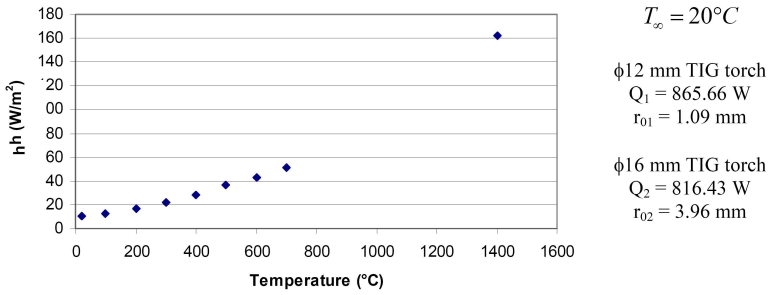

Fig. 6 Identified values of convection-radiation coefficient and heat source parameters.

sured and numerically simulated time evolutions of the temperature at different locations on the surface of the disk -in fact the locations of the thermocouples-.

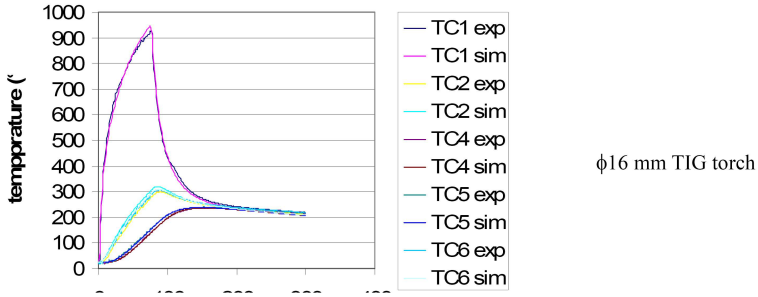

Fig. 7 Experimental vs. simulated time evolutions of temperature at the thermocouples locations.

THERMO-METALLURGICAL MODEL

X10CrMoVNb9-1 MARTENSITIC STEEL

The microstructural stability of X10CrMoVNb9-1 steel is explained by its chemical composition and in particular the high percentage of chromium and the presence of vanadium and niobium (see Tab. 4).

Tab. 4 Composition of X10CrMoVNb9-1 steel (wt%) (from [6]).

C	Mn	Si	Ni	Cr	Mo	Cu	Al	S	P
0.099	0.405	0.216	0.13	8.305	0.951	0.054	0.011	0.002	0.007

Sn	As	V	Nb	Ti
0.006	0.003	0.201	0.075	0.004

The as-delivered microstructure of this material corresponds to tempered martensite.

During heating, for instance during the welding process, depending on the maximum temperature reached, this base material may transform into austenite γ, ferrite δ or liquid (see the equilibrium pseudo-binary diagram given in Fig. 8).

MODELLING OF AUSTENITIZATION OF X10CrMoVNb9-1 DURING HEATING

The martensite $\Rightarrow$ austenite diffusion transformation -i.e. the austenitization of the base material- corresponds to a bcc $\Rightarrow$ fcc phase change. If one assumes that the important specific volume variation that is associated to this phase change is directly related to the

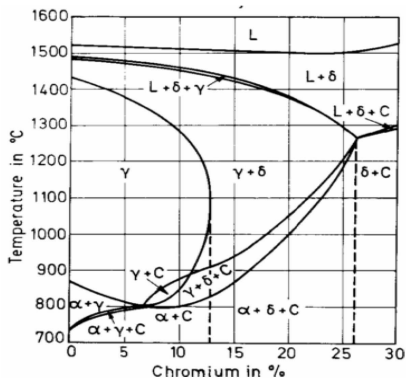

Fig. 8 Fe-0.1 wt% C/Cr equilibrium pseudo-binary diagram.

evolution of the fraction of formed austenite, this evolution of the austenite fraction rate can be identified from standard dilatometry tests, for instance at constant heating rates. Austenitization start temperature is then naturally associated to the first detection of a volume change. The evolution of the austenite fraction $y(T)$ for different constant heating rates and the corresponding plot of the austenite start temperature are given in Fig. 9a.

It has been proposed in [7] to derive from the experimental results $T(y, \dot{T})$ given in Fig. 9b the austenite transformation close to equilibrium by using a relationship proposed in [8] such that

$$T(y_{eq}) = T(y, \dot{T}) - C \left[\dot{T} T(y, \dot{T}) \exp\left(\frac{E}{R \cdot T} \right) \right]^{1/3} \tag{4}$$

In practice, for each value of austenite fraction y, $T(y_{eq})$ is identified as the average of the values computed with E [kJ/mole] $\in$ $[50, 450]$. The results are given in Fig. 10.

The approach proposed herein to model austenitization during heating assumes that the transformation can be splitted into two successive stages, viz. an incubation stage and then an initiation-and-growth stage. The complete identification of the model is a three-step process.

It has been proposed in [6] that the transformation kinetics close to equilibrium -as derived from the dilatometry tests (see Eqn. (4) and Fig. 9)- can be modelled by the following relationship

$$y_{eq}(T) = 1 - \exp\left(- \left(K_0 \left(T - A_{eq0} \right) \right)^{m_0} \right) \tag{5}$$

As proposed for instance in [9], after discretization in a set of isothermal steps Δt_i at temperatures T_i, the incubation time during any anisothermal heating $T(t)$ -for instance at a constant heating rate-, can be related to the incubation times $t_i(T_i)$ during isothermal transformation at temperatures T_i, by using Scheil additivity principle such that

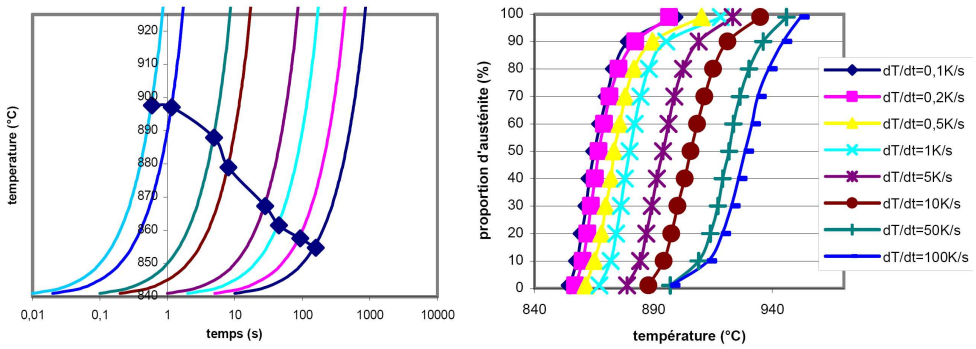

(a) Austenite start temperature. (b) Austenite transformation kinetics $y(T)$

Fig. 9 X10CrMoVNb9-1 steel (tempered martensite initial state) (from [6]).

$$\sum_i \frac{\Delta t_i}{t_i(T_i)} = 1 \tag{6}$$

Besides, it has been proposed in [10] to model the incubation times $t_i(T_i)$ with the following phenomenological relationship

$$t_i(T_i) = A(A_{ssat} - T_i)\exp\left(\frac{C}{T_i - A_{eq0}}\right) \tag{7}$$

Last, it has been proposed in [7] to model the transformation kinetics far from equilibrium -as derived from the dilatometry tests- with a modified version of a model initially proposed in [11], so that

$$\dot{y} = K\exp\left(\frac{-W}{R \cdot T}\right) \langle T(y_{eq}) - A_{eq0}\rangle_+^n (1 - y) \tag{8}$$

Eventually, this approach requires the successive identification from experimental results such as those that are given in Fig. 2-3 of the following set of parameters (A_{eq0}, K_0 and m_0), (A, A_{ssat} and C) and (K, W and n).

After identification with Matlab© (using a 4-5 order Runge-Kutta scheme with temperature steps equal to 1 °C), the complete model is apt to describe the austenitization kinetics during any anisothermal heating loading, for instance at constant heating rates as illustrated by Fig. 9.

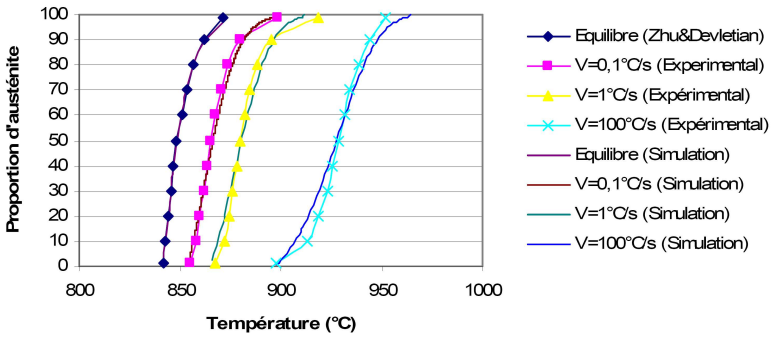

Fig. 10 Austenite transformation kinetics close to $(y - eq(T))$ and far from $(y(T))$ equilibrium X10CrMoVNb9-1 steel (tempered martensite initial state).

MODELLING OF OTHER TRANSFORMATIONS OF X10CrMoVNb9-1 DURING WELDING

In the following, as a first approximation, the austenite $\Leftrightarrow$ ferrite δ transformation is ignored.

During cooling, whatever the cooling rate (in fact such that $\dot{T} \geq 0.2$ K/s), austenized material transforms into quenched martensite. Standard Koistinen-Marburger model has been used to model this transformation so that the martensite fraction $y_m(T)$ during cooling is modelled by

$$y_m(T) = y_0 \left(1 - \exp\left(-K_m(M_s - T)\right)\right) \tag{9}$$

where y_0 denotes the initial volume fraction of the austenite that depends on the heating loading faced by each point in the vicinity of the weld, whereas K_m and M_s denote material coefficients.

NUMERICAL SIMULATION OF SIMPLE TIG WELDING TESTS

The simplified thermo-metallurgical model briefly described above has been implemented in the finite element software Cast3M. Latent heats associated to each phase transformation (martensite $\Rightarrow$ austenite, austenite $\Leftrightarrow$ (ferrite δ/)liquid and austenite $\Rightarrow$ martensite) are taken into account during heat transfer analyses without specific treatment of the molten zone.

An illustration of the result of the simulation of a disk-spot TIG welding test is given in Fig. 11 where experimental and simulated heat affected zones may be compared. One can notice that the size of the molten zone is underestimated by the numerical simulation: this point can be explained by the fact that the austenite $\Leftrightarrow$ ferrite δ transformation has been ignored and that the exact values of the liquidus and solidus temperature are yet unknown for the material brand used for these experiments. Besides, it can be noticed that the ferrite δ not only appears during heating but is still present in non-negligible proportions after cooling. Last, it can be noticed that the quenched martensite in the heat

affected zone exhibits two clearly different morphologies: this point may be related with phenomena that have not been discussed herein, viz. carbides dissolution and austenite grain growth.

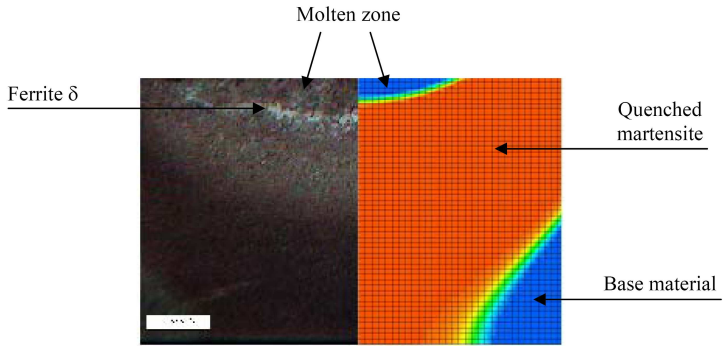

Fig. 11 Microstructure of the heat affected zone (experimental vs. simulated).

An illustration of the result of the simulation of a DISK-CYCLE test is given in Fig. 12.

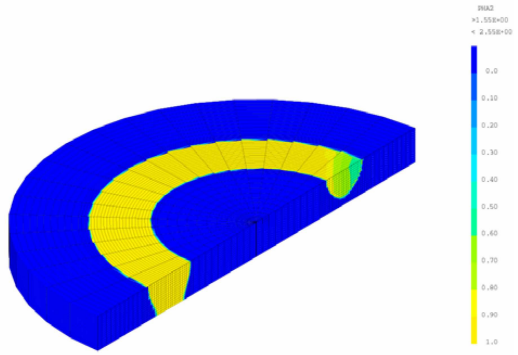

Fig. 12 Austenite fraction simulated during a disk-cycle TIG welding test.

CONCLUSIONS AND WORK IN PROGRESS

The identification procedure of the thermal boundary conditions that is presented in this paper has been first implemented while using temperature measurements from thermocouples located in six different points of the disk (see Fig. 1). A similar procedure is currently being developed while replacing the temperature measurements from thermocouples TC1, TC2 and TC3 by a temperature field measured by an IR camera.

The results that are briefly discussed in the last section of this paper prove that the thermo-metallurgical model that is presented in this paper can be improved, in particular

to take account of the austenite $\Leftrightarrow$ ferrite δ transformation, carbides dissolution, austenitic grain growth and thermo-metallo-mechanical couplings.

During multi-pass welding process, after reheating induced by successive welding passes, transformed material may be as-delivered material i.e. tempered martensite or quenched martensite resulting from previous pass(es). Besides, depending on the maximum temperature reached, quenched martensite may be austenized or only tempered. These complex loadings require further investigations in terms of thermo-metallurgical model.

REFERENCES

[1] RCCMR, CEA, 2002.

[2] G.M. Roux and R. Billardon: 'Identification of Thermal Boundary Conditions and Thermo-Metallurgical Behaviour of X10CrMoVNb9-1 Steel. Application to a Disk-Spot Welding Experiment', *Journees SNS*, AFM, La Défense, Paris, pp. 24-27, 2006.

[3] K. Levenberg: 'A Method for the Solution of Certain Problems in Least Squares', *Quart. Appl. Math.*, Vol. 2, pp. 164-168, 1944.

[4] D. Marquardt: 'An Algorithm for Least Squares Estimation of Non Linear Parameters', *Siam. J. Appl. Math.*, Vol. 11, pp. 431-441, 1963.

[5] T. Charras and J. Kichenin: 'L'Optimisation Dans Cast3M', *Rapport CEA*, DM2S/SEMT/RT/05-007/A, 2005.

[6] R. Duthilleul and J.-C. Brachet: 'Etude des Evolutions Microstructurales Lors D'Un Traitement Thermique Rapide á Haute Température D'Un Acier de Type T91', *Document Technique CEA/DMN*, 2005.

[7] J.-C. Brachet, L. Gavard, C. Boussidan, C. Lepoittevin, S. Denis and C. Servant: 'Modelling of Phase Transformations Occuring in Low Activation Martensitic Steels', *J. Nucl. Mater.*, Vol. 258-263, pp. 1307-1311, 1998.

[8] Y.T. Zhu and J.H. Devletian: 'Determination of Equilibrium Solid Phase Transition Temperature Using DTA', *Metall. Trans. A*, Vol. 22, pp. 1993-1998, 1991.

[9] E. Gautier Aeby: 'Transformations Perlitique et Martensitique Sous Contrainte de Traction Dans les Aciers', *PhD thesis*, Université de Nancy, 1985.

[10] G.M. Roux, F. Hild and R. Billardon: 'Modélisation de la Transformation Austénitique au Chauffage D'Un Acier Martensitique'. In: *Colloque National MECAMAT*, Aussois, 2006.

[11] R.A. Holt, *et al.*: *IAEA Specialists Meeting*, IWGFPT/7, Blackpool, UK, 1980.